J. Biophoton. **3**, No. 7, 462–467 (2010) / **DOI** 10.1002/jbio.200900094

Journal of BIOPHOTONICS

LETTER

High-resolution tomographic diffractive microscopy of biological samples

Bertrand Simon[1], *Matthieu Debailleul*[1], *Anne Beghin*[2], *Yves Tourneur*[2], *and Olivier Haeberlé*[*, 1]

[1] Laboratoire MIPS-EA2332, Université de Haute-Alsace, IUT Mulhouse, 61 rue Albert Camus, 68093 Mulhouse Cedex, France
[2] Centre Commun de Quantimétrie; Université Lyon 1; Université de Lyon; F-69373 Lyon, France

Received 15 December 2009, revised 17 February 2010, accepted 17 February 2010
Published online 4 March 2010

Key words: 3D microscopy, holography, tomographic diffractive microscopy, biological analysis

Supporting information for this article is available free of charge under http://dx.doi.org/10.1002/jbio.200900094

The authors have developed a tomographic diffractive microscope that combines microholography with illumination from an angular synthetic aperture. It images specimens relative to their complex index of refraction distribution (index and absorption) and permits imaging of unlabelled specimens, with high lateral resolution. The authors now study its use for biological applications, and imaged several preparations with fluorescence confocal microscopy and tomographic diffractive microscopy. The results highlight some interesting features of this instrument, which should attract the interest of biologists for this new technique.

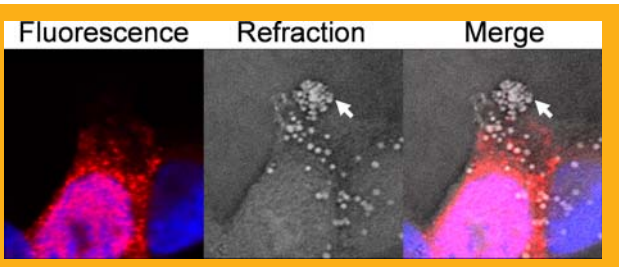

Multimodal imaging of human influenza infected A549 cells.

1. Introduction

Two main domains of biomedical research, namely virology and cancerology, make frequent use of imaging techniques such as electron and optical microscopy. At the cellular level, there are a number of organelles and structures with a size between 20 to 200 nm. The experimental resolution of confocal microscopy is about 200–250 nm and for electron microscopy, the biological sample preparation and the acquisition of 3D images are fastidious. Despite recent advances, 3D imaging and correct visualization of some cellular structures is still difficult (especially if fluorescence labelling is to be avoided) but could in some cases be performed by tomographic diffractive microscopy, which can deliver images with a resolution in the 100 nm range.

We have developed such a tomographic diffractive microscope, an emerging instrument, which combines microholography with tomography by varying the illumination direction, and that is able to deliver high-resolution images of transparent, unlabelled specimens. We describe here observations of various biological samples, highlighting some potential applications of this promising technique.

* Corresponding author: e-mail: olivier.haeberle@uha.fr, Phone: +33 3 89 33 76 11, Fax: +33 3 89 33 76 05

2. Experimental setup

Our tomographic diffractive microscope is based on the idea of Wolf [1], who proposed a technique, which from the electromagnetic field diffracted by a semitransparent specimen, permits numerical reconstruction of the index of refraction distribution within this specimen, a quantity that is hardly or simply not measurable with classical microscopes. Using a coherent illumination, this approach therefore constitutes a progress, as using incoherent light produces images presenting a contrast resulting from a complex interaction of the field and the sample, and that is, strictly speaking, adapted to morphological measurements only.

The implementation of our system is inspired by the setup proposed by Lauer [2], adapted to an Olympus IX71 inverted microscope body, and equipped with an Olympus FV300 fluorescent scanner [3, 4]. We have, in particular, demonstrated the high resolution achievable with such a technique [5].

We here just briefly recall the basic principles of tomographic diffractive microscopy, forwarding the reader interested in the theoretical and technical aspects towards Refs. [2–4] that give a detailed description of the technique.

A HeNe laser ($\lambda = 633$ nm) generates a coherent beam, which is split into an illumination wave and a reference wave that are injected into optical fibers. The illumination beam is refocused onto the back focal plane of the condenser, so that the illumination wave leaves the condenser as a plane wave.

Passing through the specimen, the illumination wave is partly diffracted. An oil-immersion objective ($100\times$, $NA_{obj} = 1.4$) collects the diffracted wave, which is refocused to form an image of the specimen onto a CCD camera. The nonscattered part of the incoming wave is also captured by the objective. The whole optical system is tuned so that this nonscattered beam impinges onto the CCD as a plane wave.

A recombination cube mixes the scattered as well as the nonscattered beams with the reference beam, also focused as a plane wave onto the detector, in order to record a hologram. The phase and amplitude of the hologram are reconstructed using a four-step phase-shifting procedure, via a piezoelectric mirror [3, 4].

Such a setup constitutes a holographic microscope. The fundamental principle of tomographic diffractive microscopy is to combine many holograms recorded with various incidences of illumination [1, 2]. The direction of the illumination wave is controlled using a tip-tilt mirror, so as to cover the full illumination angle range of the high numerical, oil-immersion condenser ($NA_{cond} = 1.4$).

The fusion of the data is performed in Fourier space, and a final 3D Fourier transform gives an image that consists of two parts, one depicting the index of refraction distribution, the other giving the absorption distribution, throughout the specimen. After proper calibration, the absolute complex index of refraction distribution is recordable [6].

Furthermore, the use of coherent light overcomes the classical Abbe limit [2, 5]. Indeed coherent light permits Fourier frequencies to be recorded without attenuation. The optical transfer function support of the tomographic diffractive microscope is the same than the optical transfer function support of a classical transmission microscope, but the latter suffers from a strong attenuation at high frequencies, resulting in less than optimal reconstruction of the small features of the image. With tomographic diffractive microscopy these high frequencies are indeed better recorded, so that the final resolution is improved. Usually, the use of coherent light in the field of classical microscopy is performed with one illumination angle only (microholography), which results in a poorer resolution. The high resolution permitted by tomographic microscopy results from the *combination* of coherent illumination (which permits recording high frequencies without attenuation) with angular scanning (which permits a synthetic aperture process at illumination).

References [1, 2, 5], to which the interested reader is referred, explain in more detail this advantageous feature of tomographic diffractive microscopy. We shall here just recall that the theoretical resolution of tomographic diffractive microscopy is $\lambda/(4\mathrm{NA})$ [2], a factor of two better than for classical incoherent transmission microscopy. For our setup, this translates into a theoretical resolution of 113 nm, and using a shorter wavelength would enable the resolution to go below 100 nm (for example, 85 nm with $\lambda = 405$ nm and using a water-immersion objective with $\mathrm{NA} = 1.2$).

Our high-resolution setup is presently slow in data acquisition. The reason is that the illumination of the specimen cannot be performed under all angles of incidence allowed by the condenser as with incoherent illumination. From an information processing point of view, the classical transmission microscope with incoherent light is a parallel information processing system, the specimen being simultaneously illuminated with all the incidence angles allowed by the condenser.

The tomographic diffractive microscope with coherent light, on the contrary, is a sequential information processing system. Indeed, it is not possible to simultaneously illuminate the specimen with coherent light with all the incidences. The incident waves would form an interference pattern corresponding to the focusing by the condenser, and it would be impossible to unravel the various Fourier components of the sample from the unique recorded hologram. For the technical reasons detailed in Ref. [3], it may take up to 40 min to acquire the 4000 holograms required for reconstruction of a high-re-

solution image [5]. We therefore in this paper limit our study to fixed specimens. The processing of the 4000 holograms (extraction of the amplitude and phase, mapping into the Fourier space, final 3D complex Fourier transform for a 512^3 voxel image takes less than 5 min on a 2.6 GHz Single Core Pentium IV with 8 GB RAM.

Choi and coworkers have, however, proven that, with an appropriate setup, this technique can deliver 3D images of living specimens [6–8]. In their experiment, attention has been focused toward speed of acquisition and absolute measurements of optical indices. The results presented, however, did not highlight the high resolution theoretically achievable with this technique [8].

3. Materials and methods

The setup described in the previous section has been used for imaging various biological specimens. Some of them (cancerous cells and virology specimens), for which we first give the materials and methods for their preparation, were also imaged with a confocal microscope.

3.1 Confocal microscopy

Fixed and immunostained cells were imaged at the Centre Commun de Quantimétrie (Lyon, Université Claude Bernard, France) using a confocal spectral microscope Leica TCS-SP2, with a 63X NA 1.32, HLX PL APO oil lens. A motorized stage was used for marking the positions of the observed fields.

3.2 Cell lines and viruses

Human mammary epithelial transformed HME-1 cells have been prepared and maintained as previously described [9]. Human respiratory epithelial carcinoma A549 cells were maintained in Dulbecco's modified Eagle's medium, supplemented with 10% fetal calf serum. All cells were maintained at 37 °C with 5% CO_2. Virus strain A/Moscow/10/99 A (H3N2) were obtained from the National Reference Center (Lyon, France). Virus stocks were cultivated in MDCK (Madin–Darby canine kidney) cells and stored at −70 °C. Virus titers were measured on MDCK cells using standard methods [10].

3.3 Matrigel cluster assay

For HME-1 cells, a cellular suspension containing 10^6 cells/µl in DMEM medium was prepared [9]. Matrigel (BD Biosciences) was added to the wells of an 8-well glass chamber slide in a volume of 300 µl. Before matrigel polymerization, 1 µl of cell preparation was carefully loaded in the middle of the matrigel coating. Then, matrigel containing preparations was allowed to solidify at 37 °C and cells formed a compact cluster. 150 µl of complete medium were then added on wells containing matrigel. After one week of culture, cell clusters were fixed in Bouin's solution and were dehydrated with alcohol, then immersed in xylene and embedded in paraffin. Four µm-thick slides were dried at 58 °C for 30 min in an incubator. After deparaffination and rehydration, the slides were mounted with a xylene mounting medium.

3.4 Fluorescence immunostaining

For immunofluorescence staining experiments, A549 infected cells have been prepared as described in Ref. [10]. The cells were fixed with formaldehyde (4% [vol/vol] in PBS) for 30 min and permeabilized with 0.1% Triton X-100 in PBS (PBST) for 15 min. Primary antibodies were diluted in PBST. Mouse anti-Nucleoprotein (17C2; gift from O. Ferraris, CNRS FRE 3011, Lyon) monoclonal antibodies were used at a 1/100 dilution in PBST. After 1 h incubation, the coverslips were washed in PBST and incubated with goat anti-mouse Alexa Fluor 633 for 30 min, at concentrations recommended by the suppliers. Nuclei were counterstained with DNA-binding fluorochrome 4,6-diamidino-2-phenylindole (DAPI, Invitrogen). After staining, the coverslips were mounted with Fluoromount G (Cliniscience).

4. Results

We now present some results obtained on biological samples with our tomographic set-up. In Fig. 1, we show cross sections of 3D images of (a) refractive index and (b) absorption distributions obtained from epithelial cheek cells. The sample was obtained from a cheek smear, diluted into a water droplet and put between a glass slide and a coverslip. A high $NA = 1.4$ oil-immersion objective and condenser were used. Because the sample is embedded in water, this value is in practice reduced to 1.33. These images have been obtained with 1000 angles of illumination, covering the full range of the condenser.

A detailed observation shows that identifiable structures are different depending on the considered quantity. The comparison between the image of refractive index and absorption permits two populations of vacuoles to be distinguished, some acting as dephasing-only elements, while others exhibit a

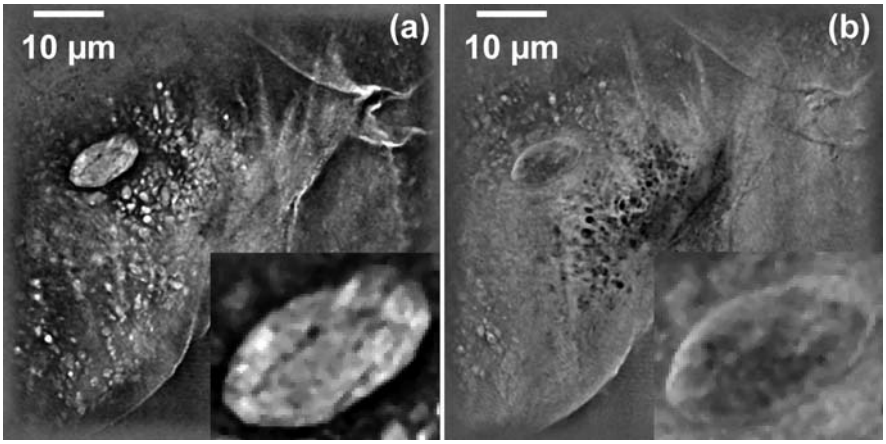

Figure 1 Epithelial cheek cells observed with tomographic diffractive microscopy. (**a**) optical index and (**b**) absorption (uncalibrated grey levels).

strong absorption. Vacuoles store materials such as glycogen or fat to be used for energy [11]. Those vacuoles that appear in white in Figure 1a are characterized by a higher index of refraction, indicating that they probably contain lipids (which are known to have a higher index of refraction than the surrounding cytoplasm), while those vacuoles that appear in black in Figure 1b are characterized by a higher absorption, indicating that they may contain the proteinic pigments, which are responsible for light absorption. This shows that, even if uncalibrated, tomographic diffractive microscopy can highlight structural differences that are otherwise difficult to detect. The enlargements highlight structures within the nucleus, which remain to be identified These observations are compatible with the complex morphology and composition of the nucleus, which often presents a varying distribution of protein or a varying DNA density, inducing refractive-index variations.

Figure 2 shows cross sections of 3D images of absorption (a) and the refractive index (b) images of polynuclear blood cells. This sample was obtained by putting a blood droplet between a glass slide and a coverslip, following the same acquisition protocol as for Figure 1. In the center of these images one can recognize a granulocyte, a polynuclear cell. The nuclei can be easily observed on the absorption cross section, while the cytoplasm is more visible on the refractive-index image. Combining both images allows these different cell elements to be distinguished without labelling, simply by their optical-property differences (see also associated video).

Figures 3, 4 and 5 show results obtained from biomedical research laboratory preparations.

Growth and morphogenesis of epithelia are essential processes in the development of many organs, which are driven not only by an intrinsic genetic program but also by signals provided by neighboring cells and tissues. Therefore, techniques of three-dimensional seeding of epithelial cells within extracellular matrix were developed and are now used in many areas (embryology, cell biology, oncology, etc.). Here, human mammary epithelial transformed cells were seeded in extracellular matrix Matrigel® to allow for the formation of 3D structures, which are called pseudo-acini. These differentiated structures are closely related to acini, which consist of the

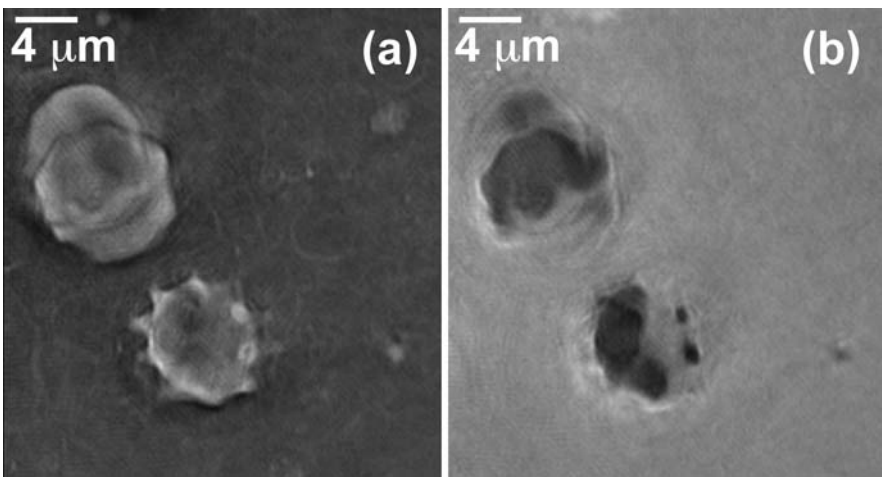

Figure 2 Granulocyte observed with tomographic diffractive microscopy (**a**) optical index and (**b**) absorption (uncalibrated grey levels) (see text and SuppInfo1.dvx).

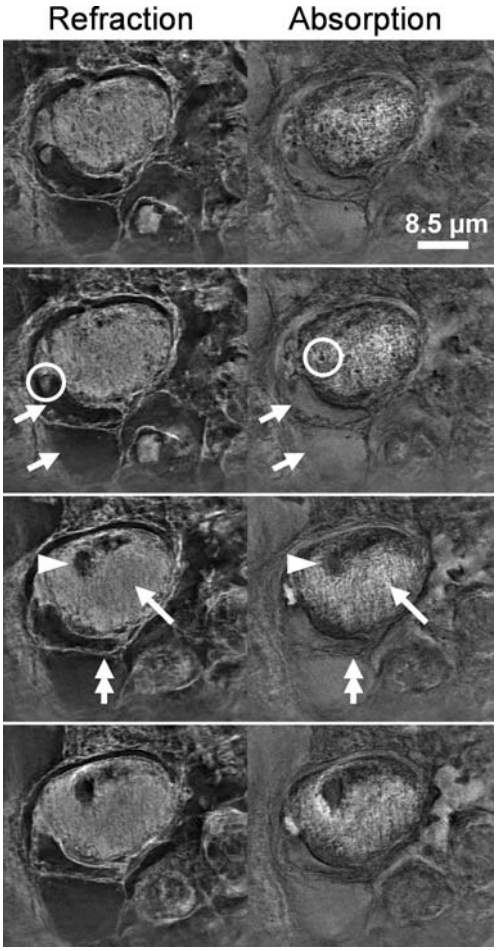

Figure 3 Human mammary epithelial transformed cells seeded in extracellular matrix (Matrigel, BD Biosciences) to allow cell differentiation and observed with tomographic diffractive microscopy (uncalibrated gray levels). Scan through successive planes along the optical axis. We identified, by morphological analogy, the nature of some structures. The white arrows (image 2) indicate probable secretion vesicles. The white arrowhead (image 3, upper) could correspond to a nucleolus, the white arrow (image 3, right) to a nucleus and the vertical double-headed white arrow (image 3, bottom) to a cytoplasmic membrane. Some others details (white circles, image 3) in secretion vesicles and in the nucleus are still undetermined.

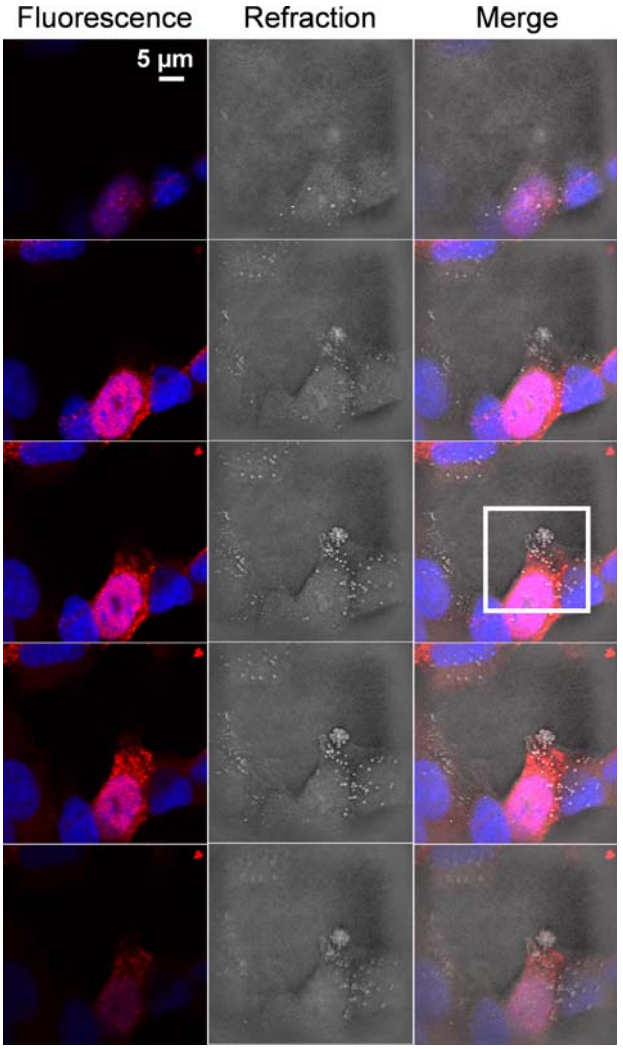

Figure 4 (online color at: www.biophotonics-journal.org) Multimodal (fluorescence confocal and tomographic diffractive microscopy) imaging of A549 cells infected with human influenza H3N2 virus (24 h after infection). Red: viral nucleoprotein NP immunostaining, Blue: DAPI staining (nucleus). Scan through successive planes along the optical axis (see text and SuppInfo2.dvx).

structural and functional elements of human breast. These structures obtained *in vitro* permits to study the effect of genetic modifications or chemotherapeutic treatments on differentiation behavior and on tumorogenesis. By using the tomographic diffractive microscope, we obtained original images and new visualization of cellular structures (Figure 3). Nucleus, nucleolus, membranes and secretion vesicles have been identified by analogical morphology. However, certain details obtained here have not yet been identified, such as some particles in the nucleus or clusters in secretion vesicles. These undetermined particles could be crucial for characterization of the cell phenotype (for milk production or proliferation for example).

In order to study impacts and damages of viral infection on cells, A549 human cells were infected with human influenza H3N2 virus and imaged with confocal microscopy. An immunostaining of the viral nucleoprotein allows infected cells to be distinguished. Using tomographic diffractive microscopy on the same cells (Figures 4 and 5 and the associated video), we observed some refracting spherical particles only present on infected cell membranes. These original structures, not observed in wide-field optical

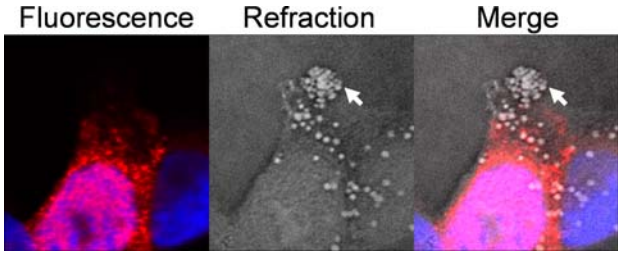

Figure 5 (online color at: www.biophotonics-journal.org) Zoom of Figure 4. The white arrow indicates spherical structures (size about 150 to 200 nm) with a clearly different optical index than others cellular structures. They could correspond to some budding of viral particles as they have been observed only on infected cells.

microscopy, but detected by electron microscopy, could correspond to budding of viral particles.

The smallest yet clearly identified spherical structures in Figure 5 have a diameter of about 160 nm, indicating that the resolution of tomographic diffractive microscopy *in a biological specimen* is (at worst) of this value, which corresponds to $\lambda/(2.8\ \mathrm{NA})$ for our setup ($\lambda = 633$ nm and NA $= 1.4$). This high-resolution capability had been up to now demonstrated only using a specially prepared carbon-mesh test pattern [5].

5. Conclusion

Using tomographic diffractive microscopy, we were able to highlight some structures not previously seen by classical optical microscopy. In particular, the possibility of differentiating structures only by their optical properties (index, absorption) represents an interesting advantage of this technique.

This new technique is to be compared with other, existing phase-constrast techniques, namely Zernike phase-constrast microscopy and differential interference contrast (DIC) microscopy, which are more familiar to biologists.

Tomographic diffractive microscopy presents three possible advantages.

First, a possibly better sensitivity with respect to absorption, resulting in a better absorption contrast (but this point remains to be effectively demonstrated).

Secondly, after a proper calibration, quantitative measurements are possible, which permits reconstruction of quantitative 3D maps of the index of refraction within microscopic specimens [6–8], as opposed to qualitative phase measurements only provided by DIC (approaches to develop quantitative DIC have also been recently proposed [12, 13]). But even if yet uncalibrated, our images show that the high sensitivity of tomographic diffractive microscopy combined with its high resolution should attract the interest of biologists willing to avoid fluorescence or contrast labelling techniques.

Finally, tomographic diffractive microscopy is an inherent 3D technique, which provides a high lateral resolution (Ref. [5] and Figure 5).

In a different work, it has also been recently shown that *reflection* tomographic diffractive microscopy permits a longitudinal resolution at least comparable to a reflection confocal microscope [14]. The successful combination of transmission and reflection diffractive tomography in a two-objective microscope [2] is still to be performed, but would open the way to microscopy of unlabelled specimen with a 3D isotropic resolution in the 100 nm range, which would represent a real breakthrough for microbiology.

We thank Dr. Manuel Rosa-Calatrava (FRE 3011, Lyon) for the preparation of the virology slide. We also thank the anonymous referees for their valuable remarks.

References

[1] E. Wolf, Opt. Commun. **1**, 153–156 (1969).
[2] V. Lauer, J. Microsc. **205**, 165–176 (2002).
[3] M. Debailleul, B. Simon, V. Georges, O. Haeberlé, and V. Lauer, Meas. Sci. Technol. **19**, 074009 (2008).
[4] B. Simon, M. Debailleul, V. Georges, V. Lauer, and O. Haeberlé, Eur. Phys. J.: Appl. Phys. **44**, 29–35 (2008).
[5] M. Debailleul, V. Georges, B. Simon, R. Morin, and O. Haeberlé, Opt. Lett. **34**, 79–81 (2009).
[6] W. Choi, C. Fang-Yen, K. Badizadegan, S. Oh, N. Lue, R. R. Dasari, and M. S. Feld, Nature Meth. **4**, 717–719 (2007).
[7] Y. Park, M. Diez-Silva, G. Popescu, G. Lykotrafitis, W. Choi, M. S. Feld, and S. Suresh, PNAS **105**, 13730–13735 (2008).
[8] Y. Sung, W. Choi, C. Fang-Yen, K. Badizadegan, R. R. Dasari, and M. S. Feld, Opt. Exp. **17**, 266–277 (2009)
[9] A. Beghin, S. Belin, R. H. Sleiman, S. Brunet Manquat, S. Goddard, E. Tabone, L. P. Jordheim, I. Treilleux, M. F. Poupon, J. J. Diaz, and C. Dumontet, PLoS One. **15**, 4(10), e7478 (2009).
[10] M. Richard, C. Deléage, M. Barthélémy, Y. P. Lin, A. Hay, B. Lina, and O. Ferraris, J. Clin. Virol. **41**, 20–24 (2008).
[11] J. G. Black, Microbiology, Principles and Explorations, 6th edn, Wiley Ed. (Hoboken, NJ, USA, 2005).
[12] S. V. King, A. Libertun, R. Piestun, C. J. Cogswell, and C. Preza, J. Biomed. Opt. **13**, 024020 (2008).
[13] S. S. Kou, L. Waller, G. Barbastathis, and C. J. R. Sheppard, Opt. Lett. **35**, 447–449 (2010).
[14] M. Sarmis, B. Simon, M. Debailleul, B. Colicchio, J.-J. Delaunay, and O. Haeberlé, "High resolution reflection tomographic diffractive microscopy", J. Mod. Opt. (accepted) DOI: 10.1080/09500341003624743.